

Charging phenomena in low-voltage electron microscopy of laser-fractured fluoride surfaces

H. Johansen

Max-Planck-Institut für Mikrostrukturphysik Halle, Weinberg 2, 06120 Halle, Germany

S. Gogoll, E. Stenzel, M. Reichling,^{a)} and E. Matthias

Freie Universität Berlin, Fachbereich Physik, Arnimallee 14, 14195 Berlin, Germany

(Received 29 April 1996; accepted for publication 30 July 1996)

Surfaces of fluoride crystals, fractured by a single excimer laser pulse and then covered by a thin conductive layer, are imaged by scanning electron microscopy in the low-voltage secondary electron mode. As a result of charging, at lower primary electron energies a contrast enhancement can be obtained for surface fragments that are no longer tightly attached to the crystal. This differs from high-energy (>10 keV) imaging which only yields topographic contrasts and allows the analysis of the fractured structure by edge and shadowing effects. Even contrast inversion from positive to negative charging of an entire fragment can be achieved, depending on the primary electron energy. It is shown that this effect can be utilized to discriminate between fragments with a good mechanical contact to the bulk and partially detached ones by systematically studying the contrast as a function of electron energy and specimen inclination. © 1996 American Institute of Physics. [S0021-8979(96)06021-5]

I. INTRODUCTION

Scanning electron microscopy (SEM) is a most useful tool for investigating laser damage in optically transparent materials. Normally surfaces of these insulating materials will be covered by a thin conducting layer to avoid charging effects during imaging.^{1,2} Such a measure aims for a stabilization of a specific surface charge state rather than to work with a surface completely free of charges.³ In previous studies^{4,5} we used SEM imaging with coated surfaces for studying thermoelastic processes related to laser-induced fracture of CaF_2 surfaces. In this way, it was possible to correlate the damage morphology with damage thresholds, to study localized energy transfer in near-surface regions,⁵ and to observe bending of regularly shaped damage fragments (tiles) due to internal stress after the rapid heating and cooling cycle.⁶ In addition, we demonstrated that by low-voltage imaging⁷ it is possible to obtain high-resolution topographic and charge-related information from SEM of uncoated CaF_2 surfaces. We showed that imaging based on charging can be utilized for detecting surface modifications much below the macroscopic damage threshold of the laser-irradiated insulator surface,⁸ which are not detectable optically.

In the present contribution we report on a SEM technique capable of detecting whether surface fragments are still firmly attached to the crystal underneath, or whether they are partially or completely disengaged from the bulk. We anticipate that the question of local adhesion or detachment of tiles is closely related to subsurface structural defects such as, e.g., screw dislocations.⁹ Therefore, the analysis of fragment detachment will not only lead to a better understanding of thermoelastic processes during laser damage in crystalline insulators, but will also be of importance for a sensitive structural defect analysis in these crystals, which is essential for an improvement of crystal growing techniques.

The mechanical contact of fragments to the bulk cannot be judged by conventional SEM techniques operating at high energies (>10 keV) since these are solely sensitive to topographic contrasts. Here, we apply the method of electron-beam-induced voltage contrast (EBIVC), exploiting the fact that secondary electron (SE) emission sensitively depends on the charge state of the surface.^{10,11} Local variations of the charge translate into SE imaging contrasts.

For a given primary electron energy, the surface covered by a thin conductive layer is in a well-defined charge state. This is determined by an equilibrium between charge input by primary electrons, secondary electron emission, and charge transport by residual surface and bulk conductivity of the nominally insulating material. When a fragment is partially detached from the bulk and electrically decoupled from the conductive layer, this charge equilibrium is disturbed which, in turn, leads to a different contrast in the SE micrograph. By varying the primary energy, i.e., the penetration depth and the secondary emission, this contrast can be controlled and even inverted, permitting a detailed analysis of the local detachment structure. Such studies are especially feasible in the range of primary electron energies between the critical energies E_1 and E_2 , where the secondary electron emission coefficient is unity.^{12,13} Also, CaF_2 is particularly suited for this type of investigation because of its rather high bulk ionic conductivity¹¹ of about $10^{13} \Omega \text{ cm}$ which allows secondary electron imaging also of uncoated surfaces for energies up to 8 keV.⁷ To our knowledge the work presented here is the first report on EBIVC used for obtaining physical information about surface modifications of an insulating sample.

Our method is very similar to electron-beam-induced current (EBIC) techniques usually utilized as characterization tool in device engineering. For this purpose a semiconductor microstructure is covered by a conducting layer of some nanometer thickness and scanned with a highly fo-

^{a)}Electronic mail: reichling@matth1.physik.fu-berlin.de

cused low-voltage electron beam. By recording the EBIC in the sample, variations in local carrier transport, e.g., due to different doping levels can be recorded with sub- μm resolution.¹⁴

II. EXPERIMENTAL PROCEDURE

Measurements were performed on CaF_2 crystals ($20 \times 20 \times 6 \text{ mm}^3$) grown by the Karl Korth company, Kiel, with the Bridgman–Stockbarger method. Crystals were cleaved along a (111) plane and mechanically polished to optical quality. Surface damage was generated in air by single shots from an excimer laser with 14 ns pulse length at a wavelength of 248 nm. The spatial beam profile was of top-hat shape with an elliptical focus ($110 \times 175 \mu\text{m}^2$) at the surface. Fluences between 0.3 and 40 J/cm^2 were used. After irradiation the damaged surfaces were covered by a carbon layer of about 15 nm thickness. This ensured that during SEM imaging most parts of the surface were on ground potential, except for electrically isolated tiles that attained a well-defined uniform potential. In some cases, we intentionally removed surface fragments by a strong flow of compressed air to investigate the fractured surface beneath the detached tiles. Micrographs were taken in a field emission scanning electron microscope either in the backscattering mode at energies of typically 20 keV or in the SE mode. For the latter, the instrument was operated at primary beam energies down to 0.5 keV without bias voltage at a slow-scan frame time of 80 s. With this frame time and a typical scanned area of $60 \times 80 \mu\text{m}^2$ a surface spot of the size of the electron-beam diameter was exposed to the electron beam for a time of 20 ns. Therefore, the electron micrographs represent snapshots of the surface charge state after electron irradiation for some nanoseconds. The inclination between the surface normal and the beam of primary electrons, further on described as the specimen tilt angle, could be varied between 0° and 90° .

III. LIGHT ABSORPTION AND FRACTURE

A general result of single shot laser impact on polished surfaces of fluoride single crystals is fracturing along the natural cleavage planes. The reason is single photon absorption by electronic states located in the upper half of the band gap and subsequent heating by electron–phonon coupling. Absorbing states could be either due to impurities, color centers, or structural defect states. The latter apparently exist along dislocations and are responsible for fracture damage in the near-surface region. Evidence for this is provided by the fact that polishing induces an additional absorption and thereby heating of a surface layer with a $1/e$ thickness of about $0.3 \mu\text{m}$.⁵

In the center parts of the laser beam with constant intensity (top-hat profile), thermoelastic stress mainly acts in the vertical direction and results in cracking at a certain depth parallel to the surface.⁵ The depth is determined by the elastic limit of the crystal which must be overcome by thermal expansion.⁶ In contrast, the strong lateral thermal gradient at the rim of the beam profile preferentially induces cracks across the surface. Therefore, the typical morphology of a laser-damaged spot on fluorides is governed by a high den-

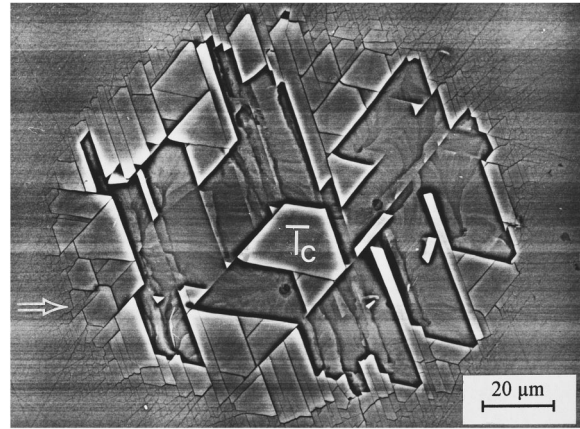


FIG. 1. Typical damage morphology on a CaF_2 -(111) surface after irradiation with a single shot of 248 nm laser light at a fluence of 27.6 J/cm^2 . The micrograph recorded in the composition mode shows backscattered electrons at 20 keV and 0° specimen tilt. T_c denotes a fragment which can be charged by the scanning electron beam.

sity of cross cracks at the periphery and large fragments, alternatively called tiles, in the center,¹⁵ as can be seen in the survey micrograph of Fig. 1. Many of the larger fragments are partially or completely detached, and the detachment base reveals a subsurface damage structure reminiscent of the (111)-plane orientation of the surface tiles. Occasionally, however, more complicated structures such as, for example, circular holes appear that are most likely the result of absorption by structural defect centers along helical dislocations.

IV. FRAGMENTS AS CHARGED MICROCAPACITORS

Figure 1 was obtained in the backscattering composition mode at a primary energy of 20 keV and shows only a weak topographical contrast. All fragments result in about the same electron scattering signal. In contrast, in a secondary electron micrograph obtained at a primary energy of 0.5 keV, i.e., at an energy below the upper critical value E_2 with a total emission coefficient $\sigma=1$,¹² some tiles exhibit a distinctly different behavior. This is demonstrated in Fig. 2,

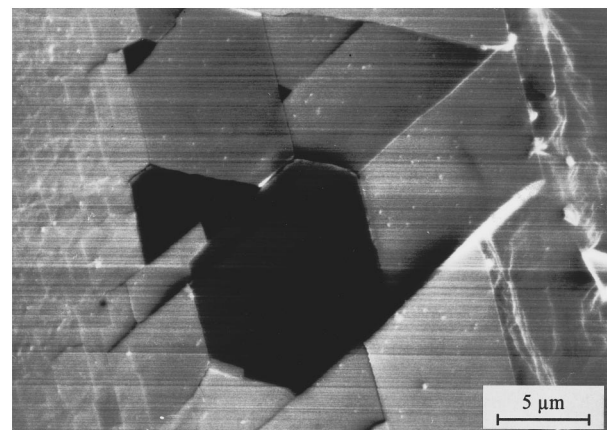


FIG. 2. Magnified detail of the marked area in Fig. 1. The micrograph was taken in the SE mode at 0.5 keV with 0° specimen tilt. Dark areas represent positively charged fragments near the periphery of the laser spot.

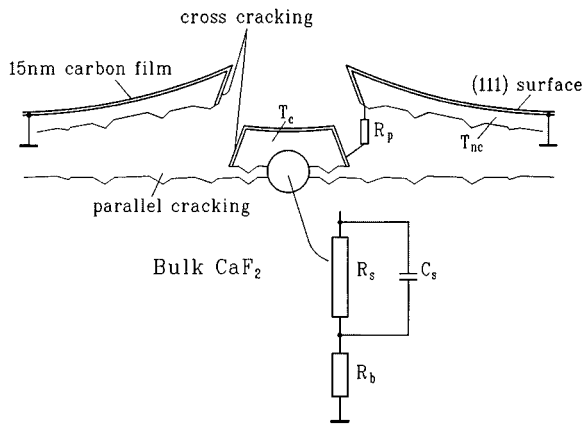


FIG. 3. Schematic cross section of the laser-fractured CaF_2 surface with chargeable T_c and nonchargeable T_{nc} tiles.

displaying the magnified SE image of the marked tiles at the left-hand side of Fig. 1. The low SE yield of the dark fragments in the center of Fig. 2 is a clear indication of a positive charge-up in this area. Imaging at various specimen tilt angles up to 70° yielded clear evidence that this contrast is due to charging and is not a result of any topographical feature.

Since the entire surface is covered by a conducting carbon layer, establishing a well-defined surface potential, charging of individual fragments implies that they are electrically decoupled from this common potential, which means mechanical separation of the carbon layer on top of the fragment from that of the surrounding surface. This situation is depicted schematically in Fig. 3. Here, a fragment labeled T_c is electrically connected to the bulk only by a large resistance R_s and isolated from the surface carbon layer (high R_p), whereas the surfaces of the nonchargeable tiles T_{nc} are in good contact with the common ground potential of the conducting layer. During scanning the quasi-insulated fragment T_c acts as a microcapacitor with capacity C_s which is charged by the primary electron beam and discharged by the bulk contact to ground (resistance R_b). Therefore, the amount of charging is governed by the mechanical contact to the bulk and determined by the effective resistance $R_s + R_b$. The polarity of the net charge depends on the coefficient for secondary electron emission, i.e., on the primary electron energy. A positive charge will result at low energies where the electron penetration depth is small and backscattering as well as secondary emission dominate. At high energies, electrons penetrate much deeper into the insulator¹⁶ which leads to a negative net charge of the fragment. As is demonstrated in the following, observing charge contrasts as a function of the primary electron energy and tilt angle of the crystal surface yields information about the mechanical attachment of the tiles.

Charging of such free-standing tiles, which is reflected by the electron-beam-induced voltage contrast, appears to be independent of scanning speed in the range 0.02–80 s per frame. It seems to be solely determined by fragment capacity and beam voltage. This means that for all scanning speeds the tiles are charged to an equilibrium level determined by

the primary electron current, the capacity, and the effective resistance $R_s + R_b$. To estimate the capacity of a T_c tile we assume an effective bulk counter electrode of the same area as the one observed under EBIVC imaging conditions; in our case, $F_t \approx 5 \mu\text{m}^2$. Using a typical fragment thickness of $0.5 \mu\text{m}$ and the relative dielectric constant of CaF_2 ($\epsilon_r = 6.81$) the capacity amounts to 10^{-15} F. If the conductivity is negligible and the tile is charged up to a typical beam voltage of 0.5 kV, the accumulated charge is approximately 10^{-12} C. These values for capacity and stored charge are quite similar to those of trench cells used for semiconductor memory devices,¹⁷ however, such cells have smaller dimensions and the capacity is realized by a much thinner insulation layer between the electrodes than in the case of CaF_2 fragments.

In contrast to our considerations for free-standing fragments, Le Gressus and Blaise¹⁸ observed a pronounced charging of grain boundaries of polycrystalline Y_2O_3 which was strongly influenced by the scanning speed in the range 5–50 s per frame. In their case, closely packed microcrystals could exchange charge through the grain boundaries. Therefore, charging was determined by the leakage current of a single grain boundary which sensitively depended on the dwell time of the electron beam. A situation similar to the one discussed by Le Gressus and Blaise¹⁸ can be seen in Fig. 2 where the varying charge contrast of the three upper fragments surrounding the free-standing center one indicates finite leakage currents.

V. CHARGE-CONTROLLED IMAGE CONTRAST

Figure 4 presents an example for a charge-induced contrast in T_c -type tiles with a comparatively strong contact to ground potential. The micrograph in Fig. 4(a) was obtained with a primary energy of 1 keV. It is not immediately evident that the strong contrast of the three triangles in the center is due to charging since the dark shading could also be interpreted as a result of shadowing. However, as shown in Fig. 4(b) the strong contrast vanishes when imaging at 8 keV. Therefore, shadowing can be excluded. The faint bright lines at the top of the triangles marked in Fig. 4(b) also yield evidence that the triangular tiles are not missing but that instead the surrounding tiles are elevated due to their internal stress. These lines are caused by enhanced emission at the edges of the triangles. The charged triangular tiles are surrounded by other fragments and presumably have a strong mechanical contact to the bulk material. Therefore, there is also a relatively good electrical contact to the surroundings and further increasing the electron energy does not change the contrast.

The situation is markedly different for the large tile in the center of Fig. 1, marked T_c . Figures 5(a) and 5(b) show the same magnified area imaged with a large tilt angle at 0.7 and 5 keV, respectively. The trapezoidal center fragment exhibits a complete contrast reversal. For the rest of the surface there is only a slight variation in shading and a general enhancement of the edge contours for 5 keV energy in Fig. 5(b). In micrographs taken at higher energies (not shown here) the center tile appears even brighter due to its strongly negative charge state.

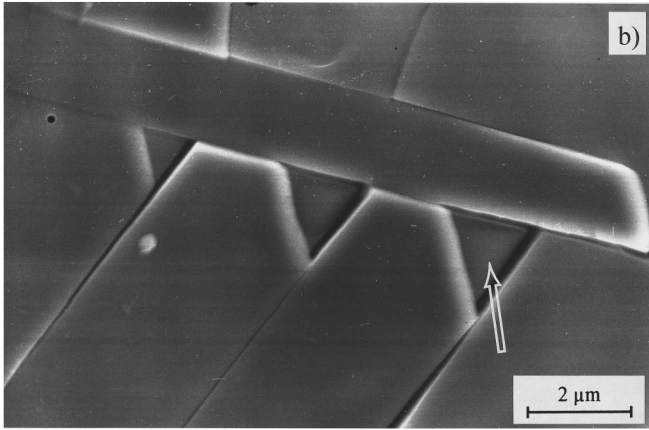
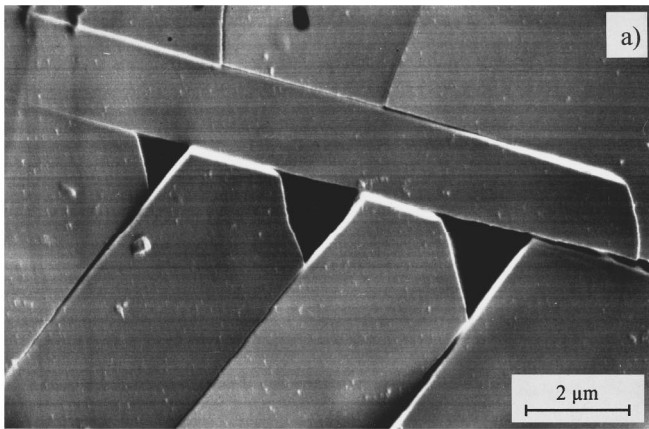


FIG. 4. Row of three triangular chargeable tiles with a relatively good mechanical contact to the bulk. Both micrographs were taken in SE mode with 0° specimen tilt and electron energies of (a) 1 keV and (b) 8 keV, respectively.

Figures 5(a) and 5(b) do not provide direct information about the degree of attachment of the trapezoidal fragment to the bulk and the effective contact area. From the charging behavior, however, we expected that the tile was only loosely bound to the bulk. It was of interest to prove this by inspecting the topography of the surface underneath. In fact, it was easy to remove the tile by an air jet. A micrograph of the fractured crystal beneath the trapezoidal fragment is shown in Fig. 6. Apparently the tile was originally fixed by a circular feature of $2\ \mu\text{m}$ diameter near the center. In this area we also found indications for melting, while the major parts of the previously covered surface exhibit the usual pattern of step edges typical for cracking due to thermoelastic stress. Because of the circular shape of the adhesion center and the swirl structure of the surrounding step edges we propose that a helical dislocation provided the structural defects that caused the initial absorption of laser light. This rather localized absorption and heating led to a strong thermoelastic stress resulting in shock-wave generation, cracking, and finally a detachment of the whole tile. In the absorption center, however, the temperature exceeded the melting point for a short time. The resolidified material in this area then caused a local adhesion to the bulk and prevented the ejection of the tile. While this scenario is a hypothesis at the present stage

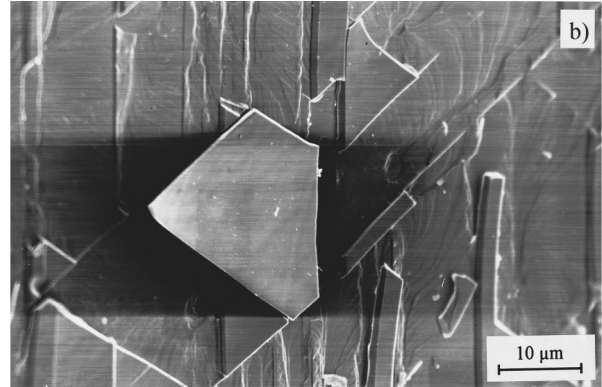
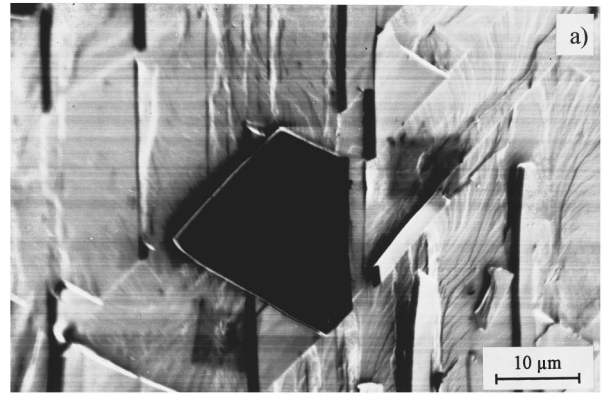


FIG. 5. Electron-beam-induced charge inversion of the fragment T_c in the center of Fig. 1 which has a weak mechanical contact to the bulk. Micrographs were obtained in SE mode at 41° specimen tilt. (a) A positive charge could be obtained at 0.7 keV and (b) a negative charge at 5 keV.

of investigations, we found supporting evidence in a number of other micrographs not shown here.

We investigated a good number of samples and varied over large ranges both the primary electron energy and the tilt angle of the specimen. Generally, we found that an optimum contrast variation for very loosely bound tiles can be obtained by variation of electron energy, while for tiles with a tighter contact to the bulk changes in contrast could be

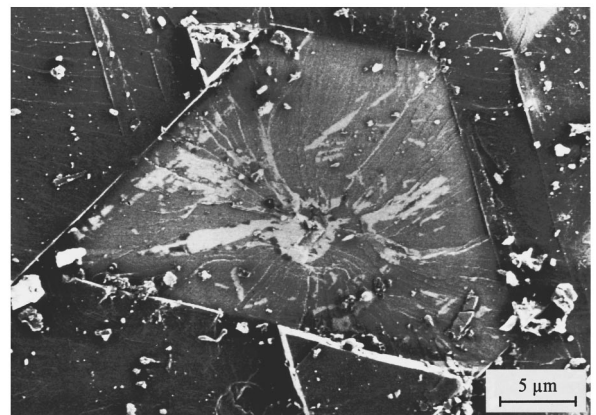


FIG. 6. Crystal topography beneath the trapezoidal fragment shown in Fig. 5 imaged at 1 keV with 0° specimen tilt. The circular feature near the center is assumed to have been the contact area of the tile prior to removal.

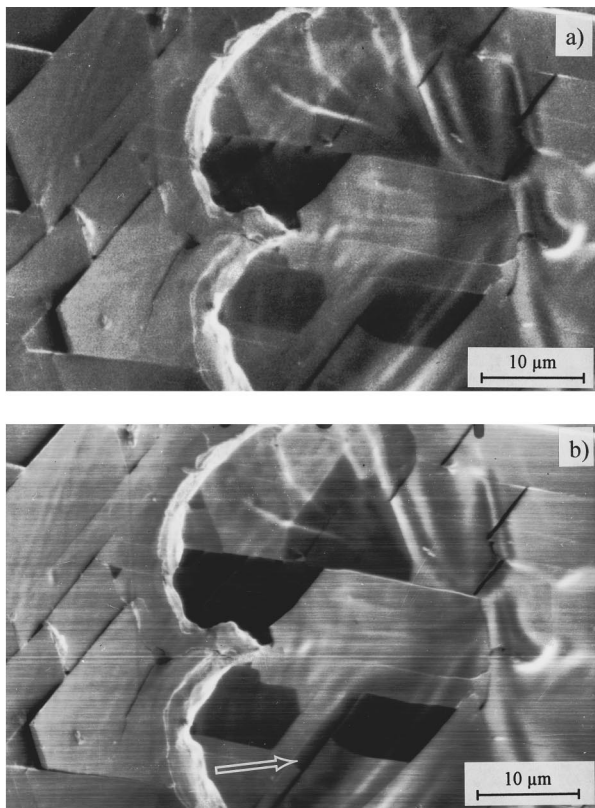
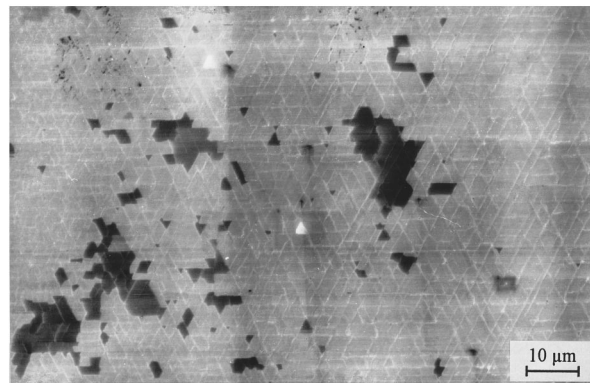


FIG. 7. Changes in SE contrast when varying the tilt angle of the specimen. The micrographs obtained at a primary energy of 0.7 keV show the same area of a laser-damaged spot on $\text{CaF}_2(111)$ irradiated with a single pulse of 20.7 J/cm^2 at 248 nm. The marked fragment exhibits the strongest change in contrast when changing the tilt angle from (a) 21° to (b) 22.5° .

better observed by varying the tilt angle. Figures 7(a) and 7(b) show an example for the sensitivity that can be obtained in the latter case. In the two micrographs the same spot on a CaF_2 surface, damaged by a fluence of 20.7 J/cm^2 , was imaged with 0.7 keV electrons, first at a tilt angle of 21° (a) and then again at 22.5° (b). There are significant differences in contrast for some fragments; the marked one especially cannot be distinguished from its surrounding at a 21° tilt angle while it exhibits a clear contrast in the micrograph taken at 22.5° . Notice that this damage spot again exhibits a semicircular fracture pattern that could be attributed to enhanced absorption by helical dislocations. Also discernible in the right-hand part of the picture is a feature which proves that temperatures in this area have been sufficiently high to cause plastic deformations.

So far evidence for positive charging was only found for primary energies close to the critical energy E_2 . Under certain conditions, however, this is also possible at much higher energies as demonstrated in Fig. 8(a). It shows a micrograph obtained at 5 keV of a multishot laser-damaged $\text{LiF}(111)$ surface which was coated by a 35 nm gold film. The dark areas again represent charged tiles on this surface. As a consequence of the higher mass density of the thick gold layer in Fig. 8(a) compared to a thin carbon film the primary electrons lose a considerable amount of energy before they reach the LiF surface. Figure 8(b) shows a plot of the effective



(a)

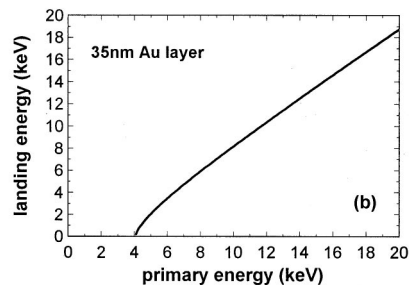


FIG. 8. (a) Dark areas indicate positive charging by 5 keV primary electrons of T_c tiles on a laser-cracked $\text{LiF}(111)$ surface covered by a 35-nm-thick Au layer. White triangles result from fragments that have been completely removed after deposition of the gold layer. The uncoated areas easily charge and exhibit a strong contrast. (b) Primary electron energy dependence of the effective landing energy after passing the 35 nm Au film calculated according to Ref. 19.

landing energy as a function of primary electron energy for 35 nm gold layer thickness, calculated according to a standard energy loss model for thin films.¹⁹ It can be seen that the expected landing energy is approximately 2 keV for primary electrons of 5 keV which is close to the E_2 value for LiF at perpendicular incidence.¹² This example demonstrates that the EBIVC technique is rather universal. It offers the advantage that the energy where a significant contrast or contrast inversion occurs can be shifted to a convenient energy region by a proper choice of the coating material and thickness. The detection of the lateral distribution of such microcapacitors by EBIVC is similar to the identification of finite and infinite clusters in percolating metal films.²⁰ In this case, different charging images allow to distinguish between the state above or below the percolation threshold of thin indium films in a capacitorlike behavior using relatively high energies of the primary electrons in the 30 keV range.

VI. CONCLUSIONS

Low-voltage secondary electron imaging of laser-damaged ionic crystal surfaces covered by a conducting layer of a thickness comparable to the electron penetration depth is very sensitive to charging of mechanically loosened surface fragments. Coating the surface avoids imaging of unstable local charge states and establishes an unambiguous potential contrast of the fragment with respect to its surrounding. Scanning with electrons of primary energy below the critical

energy E_2 allows the detection of positive charge-induced contrasts amounting to less than 2% of the secondary electron signal for uncharged regions. The mechanical contact of tiles to the bulk can be investigated by a variation of the primary electron energy. For weakly bonded tiles it is possible to obtain a contrast inversion, i.e., the fragment can also be charged negatively. At a fixed electron energy the degree of adhesion can also be judged by a change of image contrast with tilt angle. Chargeable and nonchargeable tiles may be discriminated by a tilt angle variation as small as 2° .

In summary, the EBIVC method provides information about the residual adhesion of individual tiles to the bulk of the crystal. Since laser-induced detachment of fragments is determined by light-absorbing defects, EBIVC is a promising tool for the analysis of such defects and their role for detrimental laser-surface interactions.

ACKNOWLEDGMENTS

This work was supported by the Sonderforschungsbereich 337 of the Deutsche Forschungsgemeinschaft.

- ¹R. Kelly, J. J. Cuomo, P. A. Leary, J. E. Rothenberg, B. E. Braren, and C. F. Aliotta, *Nucl. Instrum. Methods Phys. Res. B* **9**, 329 (1985).
- ²R. L. Webb, L. C. Jensen, S. C. Langford, and J. T. Dickinson, *J. Appl. Phys.* **74**, 2323 (1993).
- ³M. Liehr, P. A. Thiry, J. J. Pireaux, and R. Caudano, *Phys. Rev. B* **33**, 5682 (1986).
- ⁴M. Reichling, H. Johansen, S. Gogoll, E. Stenzel, and E. Matthias, *Nucl. Instrum. Methods Phys. Res. B* **91**, 628 (1994).

- ⁵H. Johansen, S. Gogoll, E. Stenzel, M. Reichling, and E. Matthias, *Rad. Eff. Def. Sol.* **136**, 151 (1996).
- ⁶S. Gogoll, Ph.D. thesis, Freie Universität Berlin, 1996.
- ⁷H. Johansen, S. Gogoll, E. Stenzel, and M. Reichling, *Phys. Status Solidi A* **150**, 613 (1995).
- ⁸M. Reichling, S. Gogoll, E. Stenzel, H. Johansen, and E. Matthias, in *Laser-Induced Damage in Optical Materials 1995*, edited by H. E. Bennett, A. H. Guenther, M. Kozlowski, B. E. Newnam, M. J. Soileau, *Proc. SPIE*, Vol. 2714 (SPIE, Bellingham, 1996), p. 260.
- ⁹D. Hull and D. J. Bacon, *Introduction to Dislocations*, Int. Ser. Mater. Science and Technology, Vol. 37, 3rd ed. (Pergamon, New York, 1984), p. 62.
- ¹⁰H. J. Leamy, *J. Appl. Phys.* **53**, R51 (1982).
- ¹¹M. Svantner and E. Mariani, *Krist. Tech.* **13**, 1431 (1978).
- ¹²L. Reimer, U. Golla, R. Bönigler, M. Kässens, B. Schindler, and R. Senkel, *Optik* **92**, 14 (1992).
- ¹³H. Johansen, *Beitr. Elektronenmikr. Direktabb. Oberfl.* **27**, 117 (1994).
- ¹⁴H. Blumtritt and U. Werner, in *Microscopy of Semiconducting Materials 1991*, edited by A. G. Cullis and N. J. Long, *Inst. Phys. Conf. Ser. No. 117* (IOP, Bristol, 1991), Sec. 10, p. 747.
- ¹⁵S. Gogoll, E. Stenzel, M. Reichling, H. Johansen, and E. Matthias, *Appl. Surf. Sci.* **96**, 332 (1996).
- ¹⁶R. Bennowitz, D. Smith, M. Reichling, E. Matthias, N. Itoh, and R. M. Wilson, *Nucl. Instrum. Methods Phys. Res. B* **101**, 118 (1995).
- ¹⁷L. Risch, W. Sesselmann, and R. Tielert, in *Proceedings of the 17th European Solid State Device Research Conference (ESSDERC)*, Bologna, 1987, p. 757.
- ¹⁸C. Le Gressus and G. Blaise, *IEEE Trans. Elect. Insul.* **ET-27**, 472 (1992).
- ¹⁹K. F. J. Heinrich, in *Electron Beam X-Ray Microanalysis, Determination of Thickness and Composition of Thin Layers* (VNR, New York, 1981), p. 430.
- ²⁰Z. Barkay, B. Dvir, and G. Deutscher, *Appl. Phys. Lett.* **55**, 2787 (1989).